Active Damping of Rotating Positioning Platforms using Force Feedback

T. Dehaeze [1,3]**, C. Collette** [1,2]
[1] Precision Mechatronics Laboratory
University of Liege, Belgium

[2] BEAMS Department
Free University of Brussels, Belgium

[3] European Synchrotron Radiation Facility
Grenoble, France e-mail: **thomas.dehaeze@esrf.fr**

Abstract

Abstract text to be done

1 Introduction

Due to gyroscopic effects, the guaranteed robustness properties of Integral Force Feedback do not hold. Either the control architecture can be slightly modified or mechanical changes in the system can be performed. This paper has been published The Matlab code that was use to obtain the results are available in [1].

2 Dynamics of Rotating Positioning Platforms

2.1 Model of a Rotating Positioning Platform

In order to study how the rotation of a positioning platforms does affect the use of force feedback, a simple model of an X-Y positioning stage on top of a rotating stage is developed.

The model is schematically represented in Figure 1 and forms the simplest system where gyroscopic forces can be studied.

The rotating stage is supposed to be ideal, meaning it induces a perfect rotation $\theta(t) = \Omega t$ where Ω is the rotational speed in $\mathrm{rad\,s^{-1}}$.

The parallel X-Y positioning stage consists of two orthogonal actuators represented by three elements in parallel:

- a spring with a stiffness k in $\mathrm{N\,m^{-1}}$
- a dashpot with a damping coefficient c in $\mathrm{N\,m^{-1}\,s}$
- an ideal force source F_u, F_v

A payload with a mass m in kg is mounted on the rotating X-Y stage.

Two reference frames are used:

- an inertial frame $(\vec{i}_x, \vec{i}_y, \vec{i}_z)$

- a uniform rotating frame $(\vec{i}_u, \vec{i}_v, \vec{i}_w)$ rigidly fixed on top of the rotating stage. $\vec{i}_w$ is aligned with the rotation axis

The position of the payload is represented by (d_u, d_v) expressed in the rotating frame.
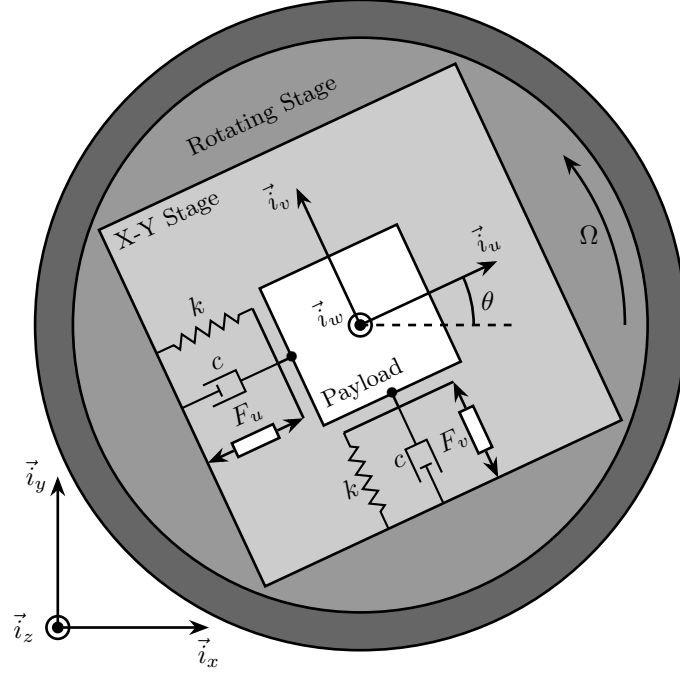

Figure 1: Schematic of the studied System

2.2 Equations of Motion

To obtain of equation of motion for the system represented in Figure 1, the Lagrangian equations are used:

$$\frac{d}{dt}\left(\frac{\partial L}{\partial \dot{q}_i}\right) + \frac{\partial D}{\partial \dot{q}_i} - \frac{\partial L}{\partial q_i} = Q_i \tag{1}$$

with $L = T - V$ the Lagrangian, D the dissipation function, and Q_i the generalized force associated with the generalized variable $\begin{bmatrix} q_1 & q_2 \end{bmatrix} = \begin{bmatrix} d_u & d_v \end{bmatrix}$.

The constant rotation in the $(\vec{i}_x, \vec{i}_y)$ plane is here disregarded as it is imposed by the rotating stage.

$$T = \frac{1}{2}m\left(\left(\dot{d}_u - \Omega d_v\right)^2 + \left(\dot{d}_v + \Omega d_u\right)^2\right) \tag{2a}$$

$$V = \frac{1}{2}k\left(d_u{}^2 + d_v{}^2\right) \tag{2b}$$

$$D = \frac{1}{2}c\left(\dot{d}_u{}^2 + \dot{d}_v{}^2\right) \tag{2c}$$

$$Q_1 = F_u, \quad Q_2 = F_v \tag{2d}$$

Substituting equations (2) into (1) gives the two coupled differential equations:

$$m\ddot{d}_u + c\dot{d}_u + (k - m\Omega^2)d_u = F_u + 2m\Omega\dot{d}_v \tag{3a}$$

$$m\ddot{d}_v + c\dot{d}_v + (k\underbrace{-m\Omega^2}_{\text{Centrif.}})d_v = F_v\underbrace{-2m\Omega\dot{d}_u}_{\text{Coriolis}} \tag{3b}$$

The constant rotation of the system induces two Gyroscopic effects:

- Centrifugal forces: that can been seen as added negative stiffness along $\vec{i}_u$ and $\vec{i}_v$
- Coriolis Forces: that couples the motion in the two orthogonal directions

One can verify that without rotation ($\Omega = 0$) the system becomes equivalent as to two uncoupled one degree of freedom mass-spring-damper systems:

$$m\ddot{d}_u + c\dot{d}_u + kd_u = F_u \tag{4a}$$

$$m\ddot{d}_v + c\dot{d}_v + kd_v = F_v \tag{4b}$$

2.3   Transfer Functions in the Laplace domain

To study the dynamics of the system, the differential equations of motions (3) are transformed in the Laplace domain and the transfer function matrix from $\begin{bmatrix} F_u & F_v \end{bmatrix}$ to $\begin{bmatrix} d_u & d_v \end{bmatrix}$ is obtained:

$$\begin{bmatrix} d_u \\ d_v \end{bmatrix} = \boldsymbol{G}_d \begin{bmatrix} F_u \\ F_v \end{bmatrix} \tag{5}$$

with $\boldsymbol{G}_d$ a 2×2 transfer function matrix

$$\boldsymbol{G}_d = \begin{bmatrix} \frac{ms^2+cs+k-m\Omega^2}{(ms^2+cs+k-m\Omega^2)^2+(2m\Omega s)^2} & \frac{2m\Omega s}{(ms^2+cs+k-m\Omega^2)^2+(2m\Omega s)^2} \\ \frac{-2m\Omega s}{(ms^2+cs+k-m\Omega^2)^2+(2m\Omega s)^2} & \frac{ms^2+cs+k-m\Omega^2}{(ms^2+cs+k-m\Omega^2)^2+(2m\Omega s)^2} \end{bmatrix} \tag{6}$$

To simply the analysis, the following change of variable is performed:

- $\omega_0 = \sqrt{\frac{k}{m}}$: Undamped natural frequency of the mass-spring system in $\mathrm{rad/s}$
- $\xi = \frac{c}{2\sqrt{km}}$: Damping ratio

The transfer function matrix (6) becomes equal to

$$\boldsymbol{G}_d = \frac{1}{k} \begin{bmatrix} \frac{\frac{s^2}{\omega_0^2}+2\xi\frac{s}{\omega_0}+1-\frac{\Omega^2}{\omega_0^2}}{\left(\frac{s^2}{\omega_0^2}+2\xi\frac{s}{\omega_0}+1-\frac{\Omega^2}{\omega_0^2}\right)^2+\left(2\frac{\Omega}{\omega_0}\frac{s}{\omega_0}\right)^2} & \frac{2\frac{\Omega}{\omega_0}\frac{s}{\omega_0}}{\left(\frac{s^2}{\omega_0^2}+2\xi\frac{s}{\omega_0}+1-\frac{\Omega^2}{\omega_0^2}\right)^2+\left(2\frac{\Omega}{\omega_0}\frac{s}{\omega_0}\right)^2} \\ \frac{-2\frac{\Omega}{\omega_0}\frac{s}{\omega_0}}{\left(\frac{s^2}{\omega_0^2}+2\xi\frac{s}{\omega_0}+1-\frac{\Omega^2}{\omega_0^2}\right)^2+\left(2\frac{\Omega}{\omega_0}\frac{s}{\omega_0}\right)^2} & \frac{\frac{s^2}{\omega_0^2}+2\xi\frac{s}{\omega_0}+1-\frac{\Omega^2}{\omega_0^2}}{\left(\frac{s^2}{\omega_0^2}+2\xi\frac{s}{\omega_0}+1-\frac{\Omega^2}{\omega_0^2}\right)^2+\left(2\frac{\Omega}{\omega_0}\frac{s}{\omega_0}\right)^2} \end{bmatrix} \tag{7}$$

For all the numerical analysis in this study, $\omega_0 = 1\,\mathrm{rad\,s^{-1}}$, $k = 1\,\mathrm{N\,m^{-1}}$ and $\xi = 0.025 = 2.5\,\%$.

Even tough no system with such parameters will be encountered in practice, conclusions will be drawn relative to these parameters such that they can be generalized to any other parameter.

2.4   System Dynamics and Campbell Diagram

The poles of $\boldsymbol{G}_d$ are the complex solutions p of

$$\left(\frac{p^2}{\omega_0^2} + 2\xi\frac{p}{\omega_0} + 1 - \frac{\Omega^2}{\omega_0^2}\right)^2 + \left(2\frac{\Omega}{\omega_0}\frac{p}{\omega_0}\right)^2 = 0 \tag{8}$$

Supposing small damping ($\xi \ll 1$), two pairs of complex conjugate poles are obtained:

$$p_+ = -\xi\omega_0 \left(1 + \frac{\Omega}{\omega_0}\right) \pm j\omega_0 \left(1 + \frac{\Omega}{\omega_0}\right) \tag{9a}$$

$$p_- = -\xi\omega_0 \left(1 - \frac{\Omega}{\omega_0}\right) \pm j\omega_0 \left(1 - \frac{\Omega}{\omega_0}\right) \tag{9b}$$

The real part and complex part of these two pairs of complex conjugate poles are represented in Figure 2 as a function of the rotational speed Ω. As the rotational speed increases, p_+ goes to higher frequencies and p_- to lower frequencies. The system becomes unstable for $\Omega > \omega_0$ as the real part of p_- is positive. Physically, the negative stiffness term $-m\Omega^2$ induced by centrifugal forces exceeds the spring stiffness k.

In the rest of this study, rotational speeds smaller than the undamped natural frequency of the system are used ($\Omega < \omega_0$).
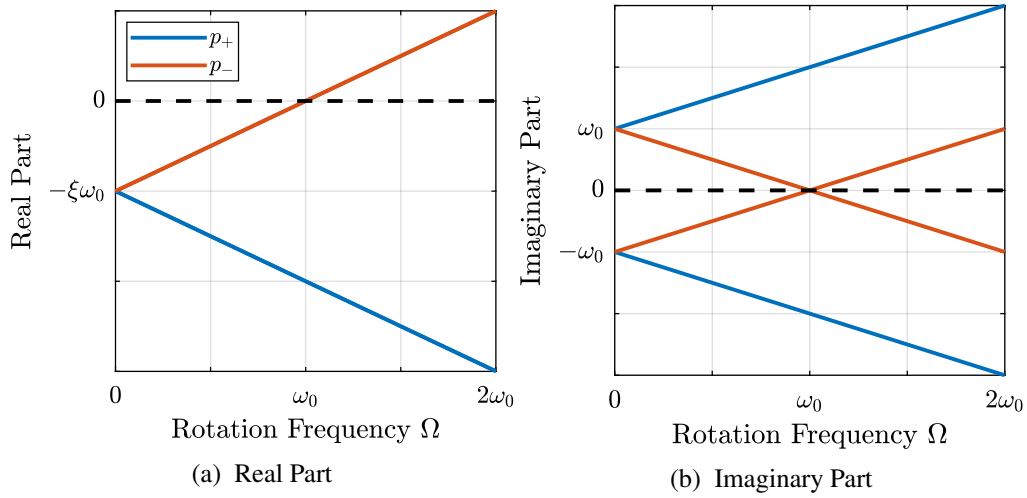

(a) Real Part

(b) Imaginary Part

Figure 2: Campbell Diagram : Evolution of the complex and real parts of the system's poles as a function of the rotational speed Ω

Looking at the transfer function matrix $\boldsymbol{G_d}$ in Eq. (7), one can see that the two diagonal (direct) terms are equal and the two off-diagonal (coupling) terms are opposite. The bode plot of these two distinct terms are shown in Figure 3 for several rotational speeds Ω.

It is confirmed that the two pairs of complex conjugate poles are further separated as Ω increases. For $\Omega > \omega_0$, the low frequency complex conjugate poles p_- becomes unstable.

3 Decentralized Integral Force Feedback

3.1 Force Sensors and Control Architecture

In order to apply Decentralized Integral Force Feedback to the system, force sensors are added in series with the two actuators (Figure 4). Two identical controllers K_F are added to feedback each of the sensed forces to its collocated actuator. The control diagram is shown in Figure 5.
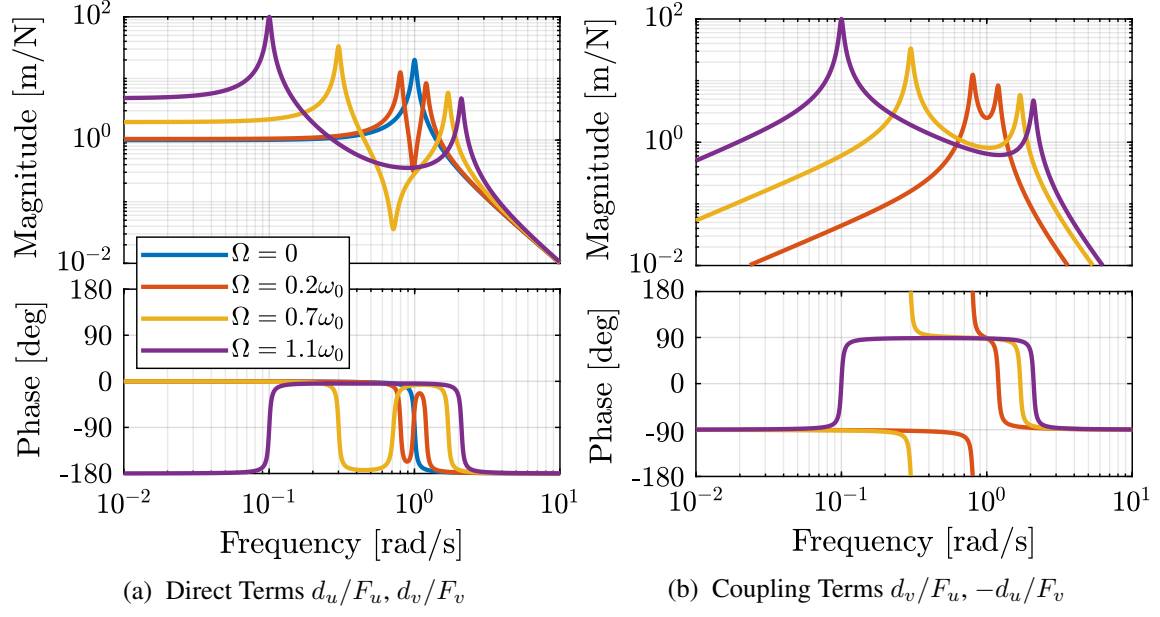
(a) Direct Terms d_u/F_u, d_v/F_v

(b) Coupling Terms d_v/F_u, $-d_u/F_v$

Figure 3: Bode Plots for $\boldsymbol{G}_d$ for several rotational speed Ω
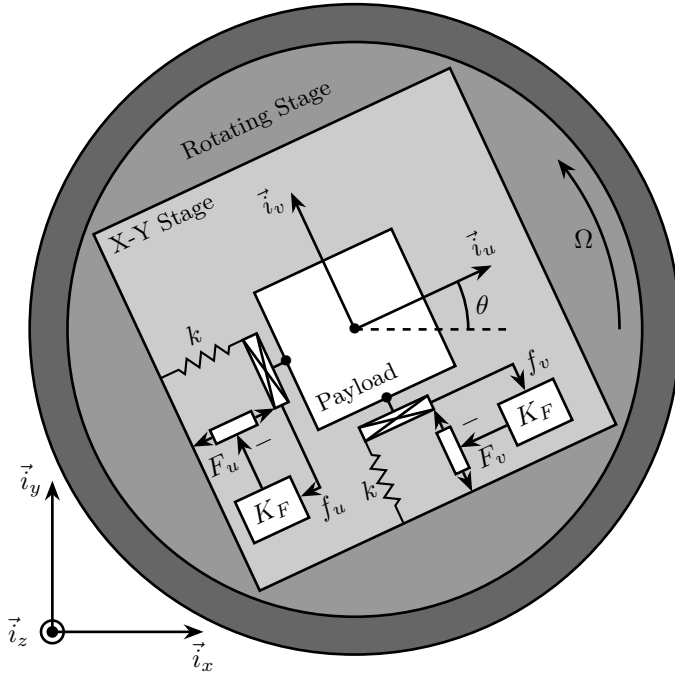

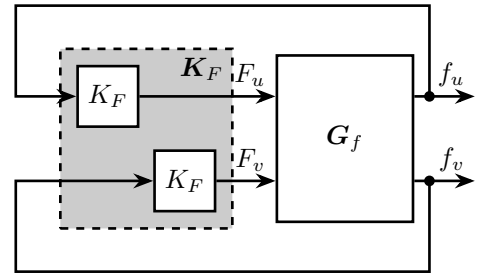Figure 4: System with added Force Sensor in series with the actuators

Figure 5: Control Diagram for decentralized IFF

3.2 Plant Dynamics

The forces measured by the force sensors are equal to:

$$\begin{bmatrix} f_u \\ f_v \end{bmatrix} = \begin{bmatrix} F_u \\ F_v \end{bmatrix} - (cs + k) \begin{bmatrix} d_u \\ d_v \end{bmatrix} \tag{10}$$

Re-injecting (7) into (10) yields:

$$\begin{bmatrix} f_u \\ f_v \end{bmatrix} = \boldsymbol{G}_f \begin{bmatrix} F_u \\ F_v \end{bmatrix} \tag{11}$$

with $\boldsymbol{G}_f$ a 2×2 transfer function matrix

$$\boldsymbol{G}_f = \begin{bmatrix} \dfrac{\left(\frac{s^2}{\omega_0^2} - \frac{\Omega^2}{\omega_0^2}\right)\left(\frac{s^2}{\omega_0^2} + 2\xi\frac{s}{\omega_0} + 1 - \frac{\Omega^2}{\omega_0^2}\right) + \left(2\frac{\Omega}{\omega_0}\frac{s}{\omega_0}\right)^2}{\left(\frac{s^2}{\omega_0^2} + 2\xi\frac{s}{\omega_0} + 1 - \frac{\Omega^2}{\omega_0^2}\right)^2 + \left(2\frac{\Omega}{\omega_0}\frac{s}{\omega_0}\right)^2} & \dfrac{-\left(2\xi\frac{s}{\omega_0} + 1\right)\left(2\frac{\Omega}{\omega_0}\frac{s}{\omega_0}\right)}{\left(\frac{s^2}{\omega_0^2} + 2\xi\frac{s}{\omega_0} + 1 - \frac{\Omega^2}{\omega_0^2}\right)^2 + \left(2\frac{\Omega}{\omega_0}\frac{s}{\omega_0}\right)^2} \\[4mm] \dfrac{\left(2\xi\frac{s}{\omega_0} + 1\right)\left(2\frac{\Omega}{\omega_0}\frac{s}{\omega_0}\right)}{\left(\frac{s^2}{\omega_0^2} + 2\xi\frac{s}{\omega_0} + 1 - \frac{\Omega^2}{\omega_0^2}\right)^2 + \left(2\frac{\Omega}{\omega_0}\frac{s}{\omega_0}\right)^2} & \dfrac{\left(\frac{s^2}{\omega_0^2} - \frac{\Omega^2}{\omega_0^2}\right)\left(\frac{s^2}{\omega_0^2} + 2\xi\frac{s}{\omega_0} + 1 - \frac{\Omega^2}{\omega_0^2}\right) + \left(2\frac{\Omega}{\omega_0}\frac{s}{\omega_0}\right)^2}{\left(\frac{s^2}{\omega_0^2} + 2\xi\frac{s}{\omega_0} + 1 - \frac{\Omega^2}{\omega_0^2}\right)^2 + \left(2\frac{\Omega}{\omega_0}\frac{s}{\omega_0}\right)^2} \end{bmatrix} \tag{12}$$

The zeros of the diagonal terms are equal to (neglecting the damping for simplicity)

$$z_c = \pm j\omega_0 \sqrt{\frac{1}{2}\sqrt{8\frac{\Omega^2}{\omega_0^2} + 1} + \frac{\Omega^2}{\omega_0^2} + \frac{1}{2}} \tag{13a}$$

$$z_r = \pm \omega_0 \sqrt{\frac{1}{2}\sqrt{8\frac{\Omega^2}{\omega_0^2} + 1} - \frac{\Omega^2}{\omega_0^2} - \frac{1}{2}} \tag{13b}$$

The frequency of the two complex conjugate zeros z_c (13a) is between the frequency of the two pairs of complex conjugate poles p_- and p_+ (9). This is the expected behavior of a collocated pair of actuator and sensor.

However for non-null rotational speeds, two real zeros z_r (13b) appear in the diagonal terms which represent a non-minimum phase behavior. This can be seen in the Bode plot of the diagonal terms (Figure 6) where the magnitude experiences an increase of its slope without any change of phase.

The low frequency gain of $\boldsymbol{G}_f$ is no longer zero, and increases with the rotational speed Ω

$$\lim_{\omega \to 0} |\boldsymbol{G}_f(j\omega)| = \begin{bmatrix} \frac{-\Omega^2}{\omega_0^2 - \Omega^2} & 0 \\ 0 & \frac{-\Omega^2}{\omega_0^2 - \Omega^2} \end{bmatrix} \tag{14}$$

This low frequency gain can be explained as follows: a constant force induces a small displacement of the mass, which then increases the centrifugal forces measured by the force sensors.

3.3 Decentralized Integral Force Feedback with Pure Integrators

The two IFF controllers K_F are pure integrators

$$\boldsymbol{K}_F(s) = \begin{bmatrix} K_F(s) & 0 \\ 0 & K_F(s) \end{bmatrix}, \quad K_F(s) = g \cdot \frac{1}{s} \tag{15}$$

where g is a scalar value representing the gain of the controller.

In order to see how the controller affects the poles of the closed loop system, the Root Locus is constructed as follows. The poles of the closed-loop system are drawn in the complex plane as the gain g varies from 0 to ∞ for the two controllers simultaneously. The closed-loop poles start at the open-loop poles (shown by ✖) for $g = 0$ and coincide with the transmission zeros (shown by ⭕) as $g \to \infty$. The direction of increasing gains is shown by the arrows ➤.

Whereas collocated IFF is known for its guaranteed stability, which is the case here for $\Omega = 0$, this property is lost as soon as the rotational speed in non-null due to gyroscopic effects. This can be seen in the Root Locus (Figure 7) where the pole corresponding to the controller is bounded to the right half plane implying closed-loop system instability.
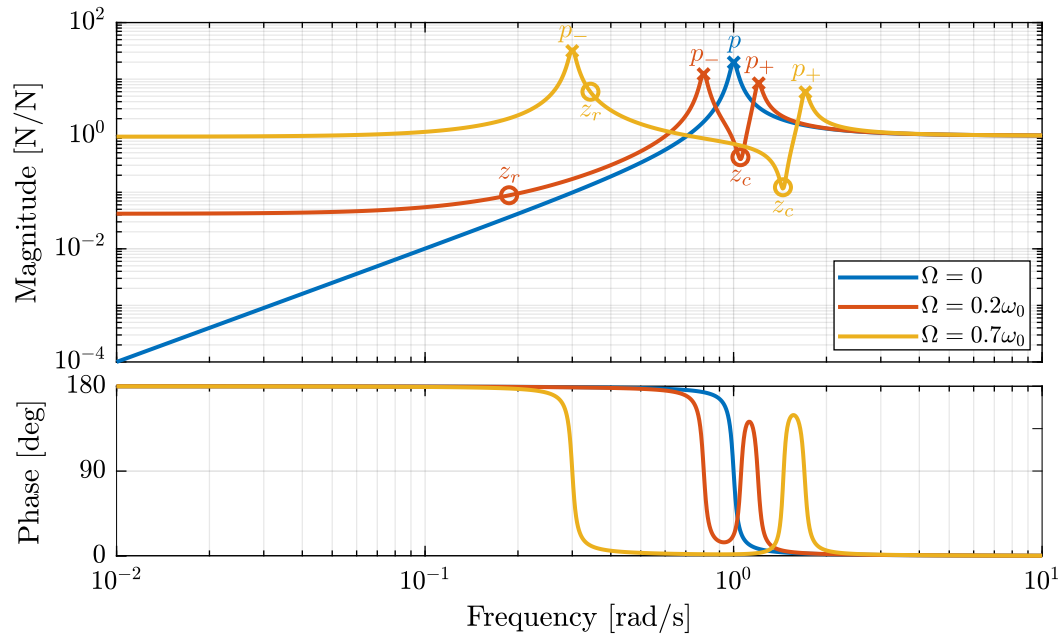
Figure 6: Bode plot of the diagonal terms of $\boldsymbol{G}_f$ for several rotational speeds Ω
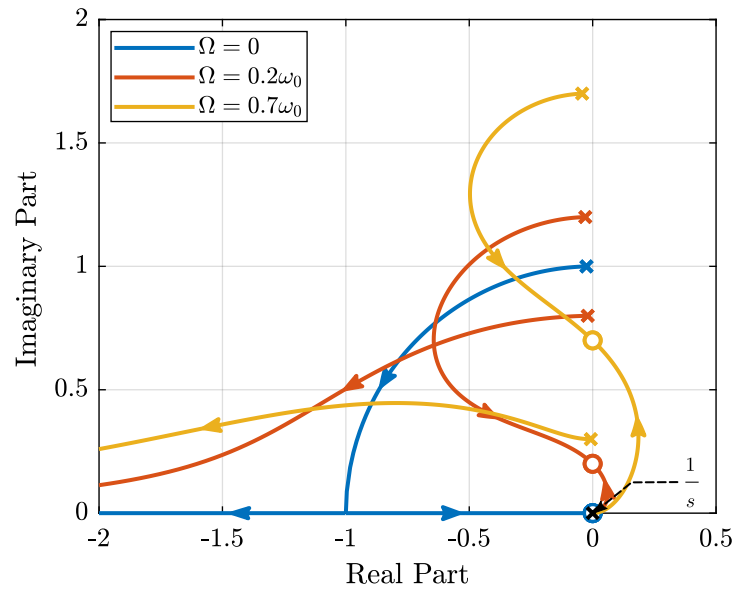

Figure 7: Root Locus for the Decentralized Integral Force Feedback

Two system modifications are proposed in the next sections to deal with this stability problem. Either the control law can be change (Section 4) or the mechanical system slightly modified (Section 5).

4 Integral Force Feedback with High Pass Filters

4.1 Modification of the Control Low

$$K_F(s) = g \cdot \frac{1}{s} \cdot \underbrace{\frac{s/\omega_i}{1 + s/\omega_i}}_{\text{HPF}} = g \cdot \frac{1}{s + \omega_i} \tag{16}$$

4.2 Feedback Analysis

Figure 8: Bode Plot of the Loop Gain for IFF with and without the HPF with $\omega_i = 0.1\omega_0$, $g = 2$ and $\Omega = 0.1\omega_0$

As shown in Figure 9, the poles of the closed loop system are stable for $g < g_{\text{max}}$

$$g_{\text{max}} = \omega_i \left(\frac{\omega_0^2}{\Omega^2} - 1 \right) \tag{17}$$

4.3 Optimal Control Parameters

Two parameters can be tuned for the controller (16), the gain g and the frequency of the pole ω_i.

Root Locus plots for several ω_i are shown in Figure 10.

The optimal values of ω_i and g may be considered as the values for which the closed-loop poles are equally damped.
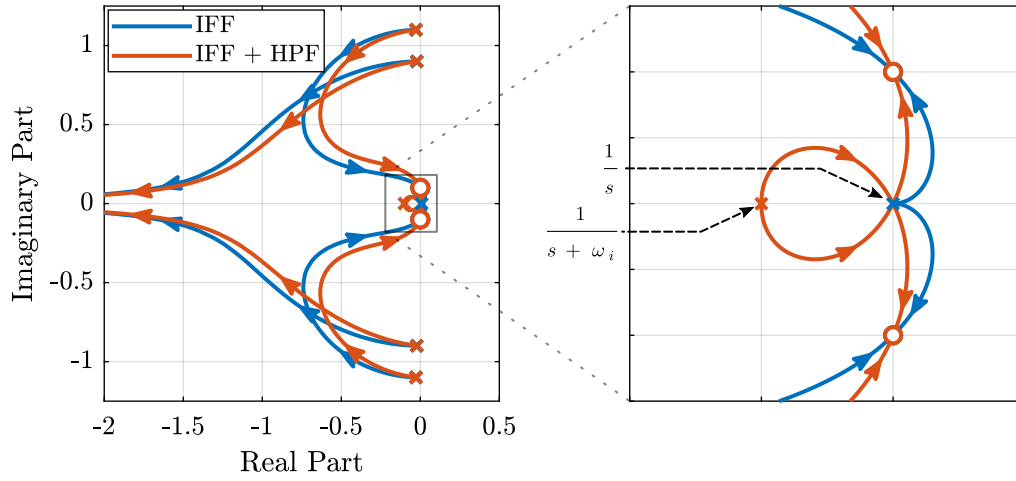
Figure 9: Root Locus for IFF with and without the HPF, $\Omega = 0.1\omega_0$
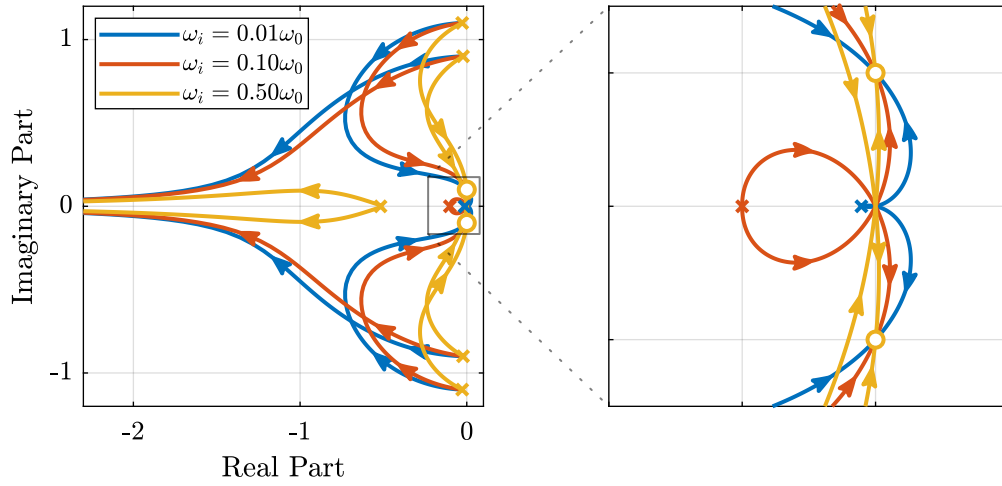

Figure 10: Root Locus for several HPF cut-off frequencies ω_i, $\Omega = 0.1\omega_0$
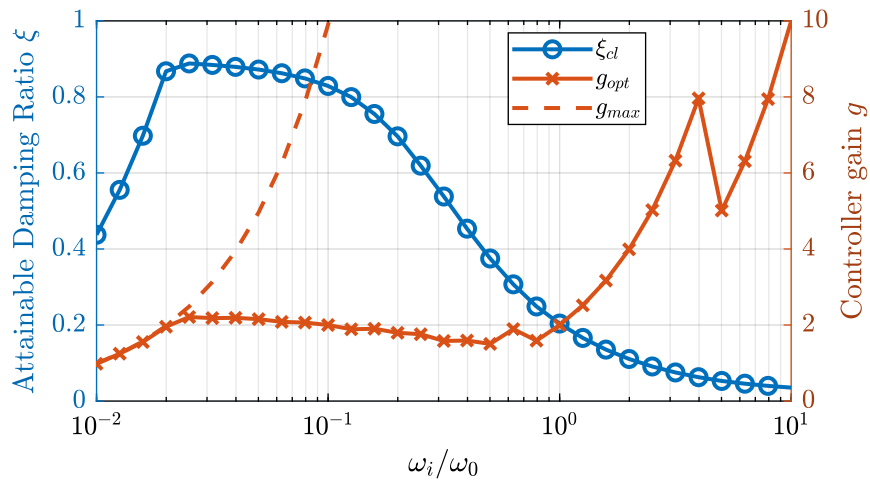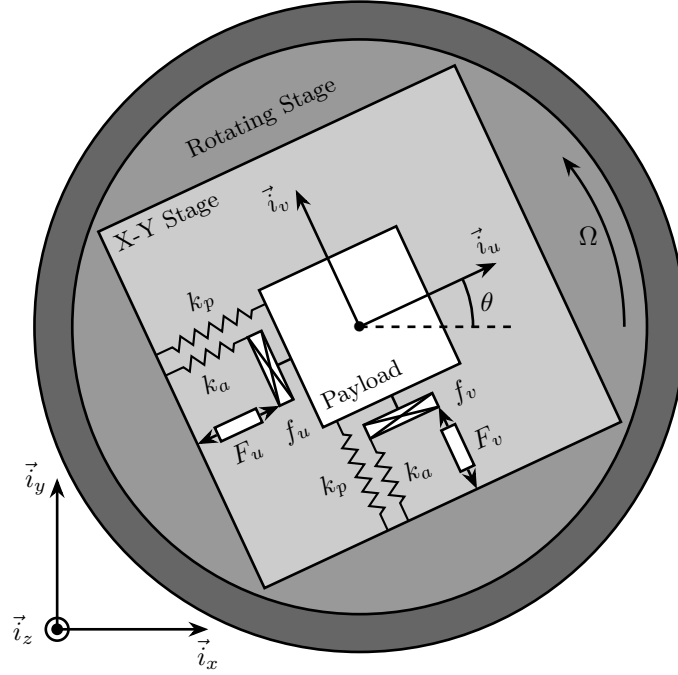

Figure 11: Attainable damping ratio ξ_{cl} as a function of the HPF cut-off frequency. Corresponding control gain g_{opt} and g_{max} are also shown

5   Integral Force Feedback with Parallel Springs

5.1   Stiffness in Parallel with the Force Sensor

Stiffness can be added in parallel to the force sensor to counteract the negative stiffness due to centrifugal forces. If the added stiffness is higher than the maximum negative stiffness, then the poles of the IFF damped system will stay in the (stable) right half-plane.

The forces measured by the force sensors are equal to:

$$\begin{bmatrix} f_u \\ f_v \end{bmatrix} = \begin{bmatrix} F_u \\ F_v \end{bmatrix} - (cs + k_a) \begin{bmatrix} d_u \\ d_v \end{bmatrix} \tag{18}$$

This could represent a system where

5.2   Plant Dynamics

We define an adimensional parameter α, $0 \leq \alpha < 1$, that describes the proportion of the stiffness in parallel with the actuator and force sensor:

$$k_p = \alpha k \tag{19a}$$
$$k_a = (1 - \alpha)k \tag{19b}$$

The overall stiffness k stays constant:

$$k = k_a + k_p \tag{20}$$

$$\begin{bmatrix} f_u \\ f_v \end{bmatrix} = \boldsymbol{G}_k \begin{bmatrix} F_u \\ F_v \end{bmatrix} \tag{21}$$

$$
\boldsymbol{G}_k = \begin{bmatrix} \dfrac{\left(\frac{s^2}{\omega_0^2} - \frac{\Omega^2}{\omega_0^2} + \alpha\right)\left(\frac{s^2}{\omega_0^2} + 2\xi\frac{s}{\omega_0} + 1 - \frac{\Omega^2}{\omega_0^2}\right) + \left(2\frac{\Omega}{\omega_0}\frac{s}{\omega_0}\right)^2}{\left(\frac{s^2}{\omega_0^2} + 2\xi\frac{s}{\omega_0} + 1 - \frac{\Omega^2}{\omega_0^2}\right)^2 + \left(2\frac{\Omega}{\omega_0}\frac{s}{\omega_0}\right)^2} & \dfrac{-\left(2\xi\frac{s}{\omega_0} + 1 - \alpha\right)\left(2\frac{\Omega}{\omega_0}\frac{s}{\omega_0}\right)}{\left(\frac{s^2}{\omega_0^2} + 2\xi\frac{s}{\omega_0} + 1 - \frac{\Omega^2}{\omega_0^2}\right)^2 + \left(2\frac{\Omega}{\omega_0}\frac{s}{\omega_0}\right)^2} \\[3em] \dfrac{\left(2\xi\frac{s}{\omega_0} + 1 - \alpha\right)\left(2\frac{\Omega}{\omega_0}\frac{s}{\omega_0}\right)}{\left(\frac{s^2}{\omega_0^2} + 2\xi\frac{s}{\omega_0} + 1 - \frac{\Omega^2}{\omega_0^2}\right)^2 + \left(2\frac{\Omega}{\omega_0}\frac{s}{\omega_0}\right)^2} & \dfrac{\left(\frac{s^2}{\omega_0^2} - \frac{\Omega^2}{\omega_0^2} + \alpha\right)\left(\frac{s^2}{\omega_0^2} + 2\xi\frac{s}{\omega_0} + 1 - \frac{\Omega^2}{\omega_0^2}\right) + \left(2\frac{\Omega}{\omega_0}\frac{s}{\omega_0}\right)^2}{\left(\frac{s^2}{\omega_0^2} + 2\xi\frac{s}{\omega_0} + 1 - \frac{\Omega^2}{\omega_0^2}\right)^2 + \left(2\frac{\Omega}{\omega_0}\frac{s}{\omega_0}\right)^2} \end{bmatrix} \quad (22)
$$

5.3 Effect of the Parallel Stiffness on the Plant Dynamics

$$
\alpha > \frac{\Omega^2}{\omega_0^2}
$$
$$
\Leftrightarrow k_p > m\Omega^2 \quad (23)
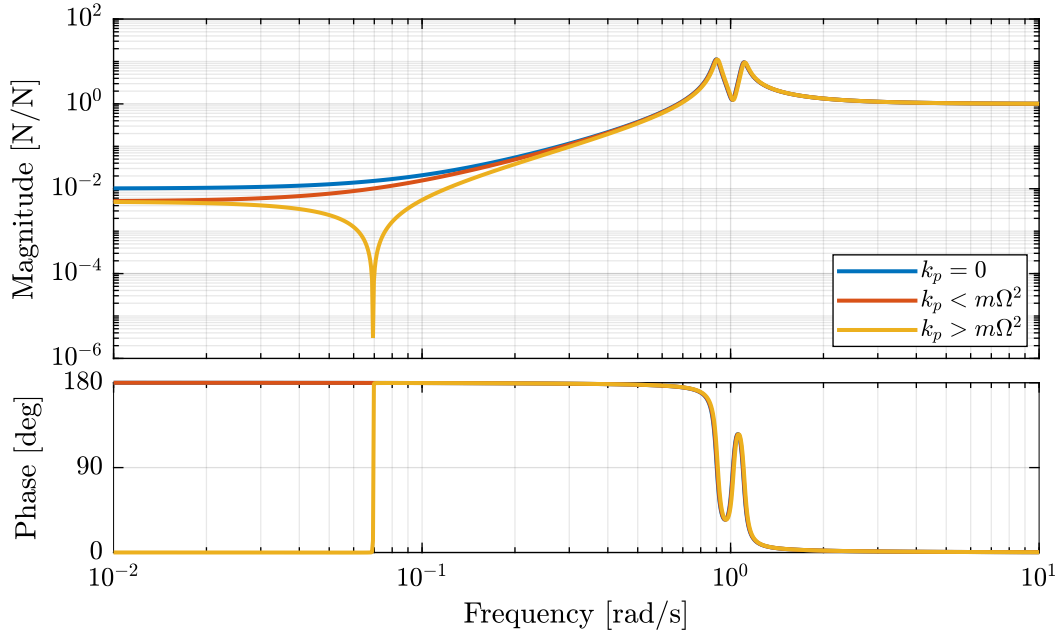$$

Figure 12: Bode Plot of f_u/F_u without parallel spring, with parallel springs with stiffness $k_p < m\Omega^2$ and $k_p > m\Omega^2$, $\Omega = 0.1\omega_0$
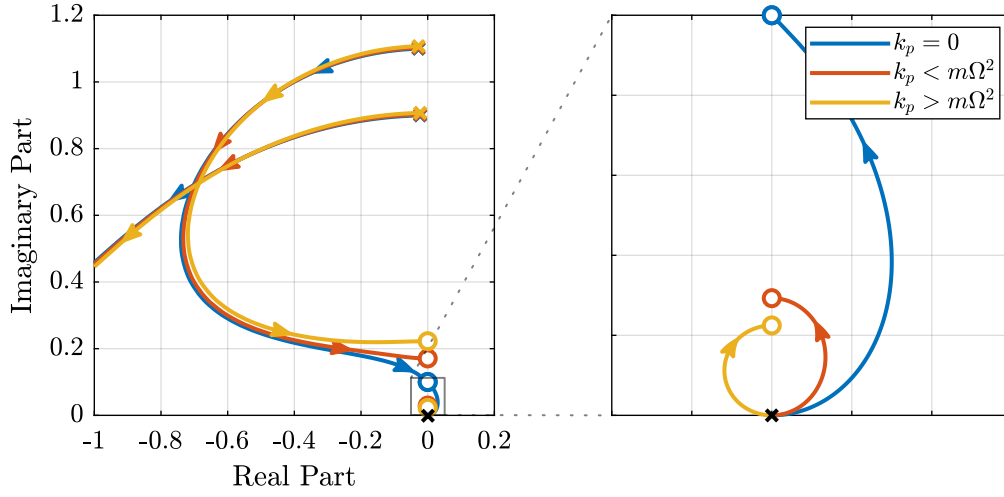
Figure 13: Root Locus for IFF without parallel spring, with parallel springs with stiffness $k_p < m\Omega^2$ and $k_p > m\Omega^2$, $\Omega = 0.1\omega_0$

(a) Three values of k_p
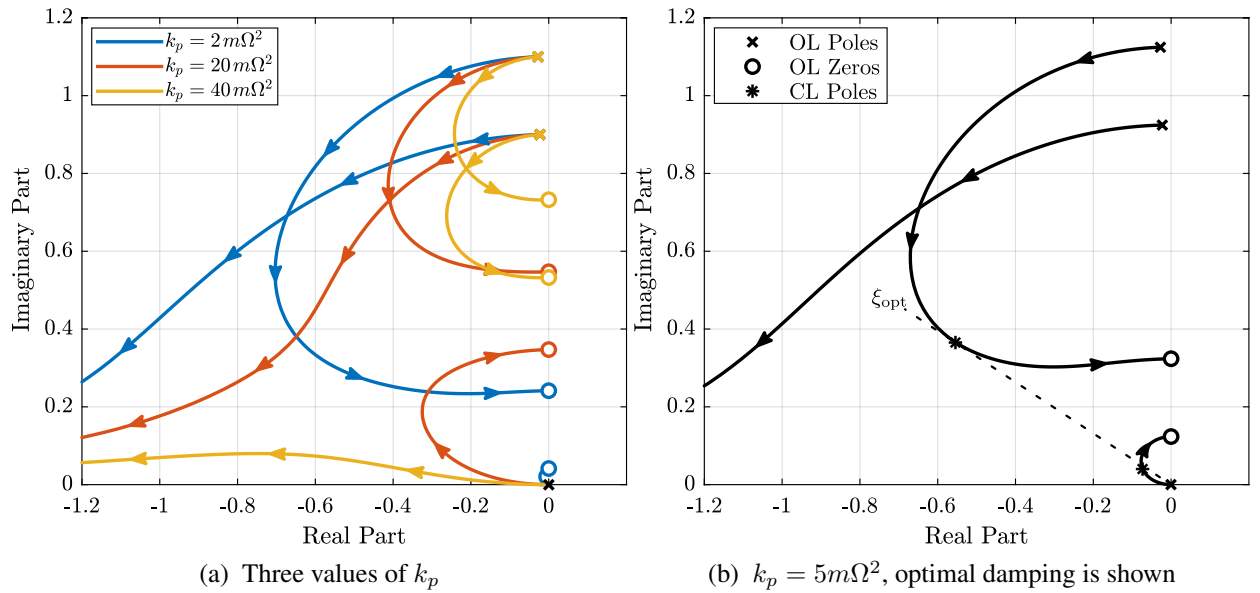
(b) $k_p = 5m\Omega^2$, optimal damping is shown

Figure 14: Root Locus for IFF when parallel stiffness is used, $\Omega = 0.1\omega_0$
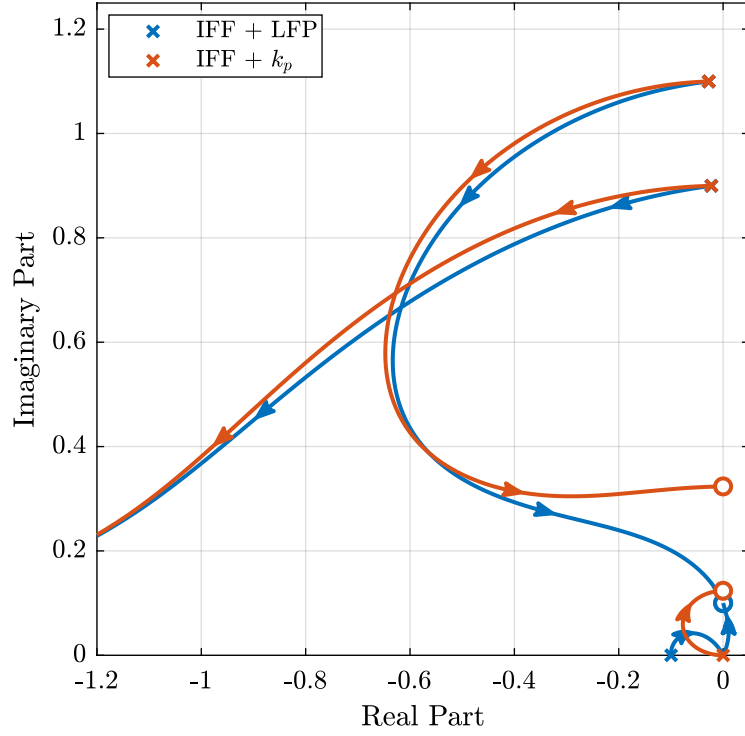
Figure 15: Root Locus for the three proposed decentralized active damping techniques: IFF with HFP, IFF with parallel springs, and relative DVF, $\Omega = 0.1\omega_0$
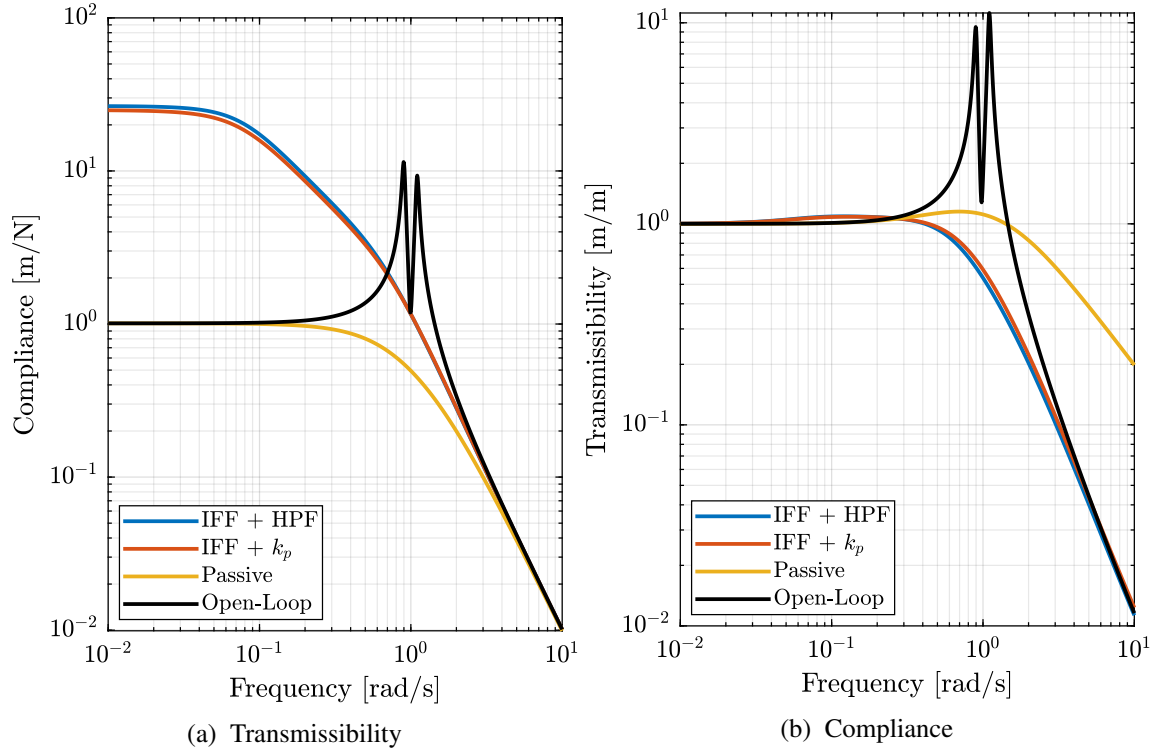

(a) Transmissibility

(b) Compliance

Figure 16: Comparison of the two proposed Active Damping Techniques, $\Omega = 0.1\omega_0$

6 Comparison of the Proposed Active Damping Techniques for Rotating Positioning Stages

7 Conclusion

Acknowledgment

References

[1] T. Dehaeze, "Active damping of rotating positioning platforms," Source Code on Zonodo, 07 2020. [Online]. Available: https://doi.org/10.5281/zenodo.3894342